Lunar eclipse brightness and the terrestrial atmosphere

Giovanni Di Giovanni

This work presents a study of the brightness of 164 lunar eclipses which were observed between 1670 and 2015. Data were analysed via four equations, which we refer to as the Formulae of Colle Leone, named after the observatory with which the author is associated. Attention is given to the quantity of ozone in the stratosphere and to the total optical depth of the atmosphere. The optical depth is correlated with both volcanic phenomena and human activities. No evidence of a correlation was found between the optical depth and solar activity.

'*La notte passata osservai l'Eclissi della* ☾ *ma però senza novità alcuna, no havendo veduto altro che quello appunto che mi ero immaginato*; *cio è che il taglio dell'ombra è indeterminantisso, et confuso…* '*

Introduction

During a lunar eclipse, the solar rays arrive in the atmosphere and are refracted by the air. They then penetrate the shadow cone of the Earth (Figure 1) and impinge on the Moon's surface. Hence, the Moon can still be seen even though it is totally immersed in the shadow cone (Figure 2).

The first rigorous theory of lunar eclipse brightness was proposed in 1933 by the Czech astronomer F. Link.[1–3] Since then, a large amount of theoretical and experimental work has been conducted in order to provide an estimation of the lunar brightness during eclipses. Recently, several methods have been developed.[4–8]

During a Lunar eclipse, the Earth's atmosphere filters the sunlight. This filtering determines the brightness and colour of the eclipsed Moon. Therefore, it is reasonable to look at lunar eclipse photometry as a useful tool to investigate air transparency and atmospheric pollution.

In general, solar radiation undergoes three different processes, which may determine its attenuation. These processes are summarised as follows:

1 Refraction: Solar ray divergence by differential atmospheric refraction;

2 Absorption: Energy absorption by water vapour and aerosols in the troposphere and by ozone in the stratosphere;

3 Scattering: If the light impinges on atoms or molecules having a smaller dimension than the wavelength of light, scattering occurs according to a process called *Rayleigh scattering* or molecular scattering. This scattering is stronger for shorter wavelengths; it is rather isotropic and it explains the blue colour of the sky. Blue light is scattered five times more than red light (See Figure 3).

Particles of aerosols and water vapour in the air are generally much larger than the wavelength of light, but solar radiation is also scattered by aerosols and water. In this case, the process differs from molecular scattering and is called *Mie scattering* or aerosol scattering. For large particles the forward scattering becomes very important; the forward scattered radiation is about a thousand times the radiation scattered backward.[9,10]

Rayleigh scattering dominates in the stratosphere, above an

* 'Last night I watched the eclipse of the [moon], but without any news, without seeing anything other than what I had imagined; namely, that the shadow is cut very indeterminate and confused…'
From the letter by Galileo Galilei to Cristoforo Clavio in Roma. *Firenze, 1610 December 30:* 'Venus and Satellites of Jupiter', (Archivio Storico, Pontificia Università Gregoriana, APUG 530 ee, 158r-159v). 'Letter written in *vulgar Italian*.'

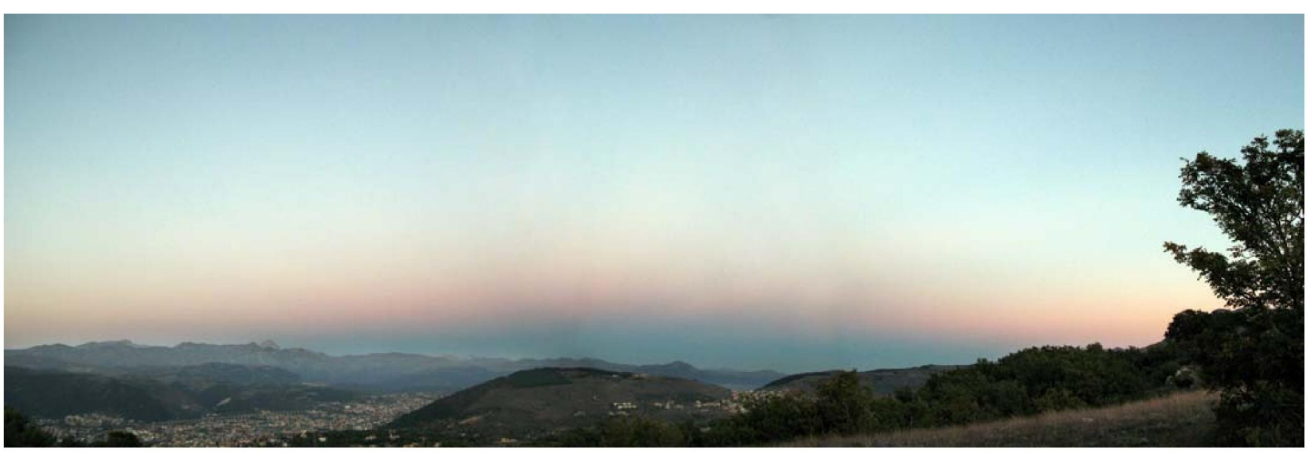

Figure 1. The Earth's shadow. Before sunrise and after sunset in the anti-solar direction a dark band rises upwards: the Earth's shadow on the atmosphere. Image 150° wide composed of three frames. The reddish halo is known as the 'Belt of Venus'. Compact camera from the top of a hill near L'Aquila city (central Italy). Twilight photometry enables amateurs to study air pollution.

Figure 2. Lunar eclipse, 2015 September 28. 15s, 150mm Newtonian, focal length 750mm; photo by Prof. Bob Gent (Cochise Skies Observatory, Arizona).

altitude of 10km. Mie scattering dominates in the troposphere, up to an altitude of almost 5km (Figure 3).

This work aims to quantify the concentration of molecular ozone (O_3) in the stratosphere and the global pollution of the terrestrial atmosphere, by using the brightness values of total lunar eclipses.

Physical background

We suppose that a light beam of intensity I_O emitted by an element of the solar photosphere is refracted in the atmosphere and undergoes an attenuation process according to Beer's law. As a result, the air transmits a divergent beam incident on the surface of the Moon with an intensity I, where:

$$I = AI_o e^{-\tau} \qquad [1]$$

where A (≈0.055) is the attenuation factor caused by the differential refraction. The product $I_o e^{-\tau}$ represents Beer's attenuation law. The exponent τ is called *optical depth* or optical thickness.[9,10] The optical depth is a quantitative measure of the opacity of the path travelled in the air by a light ray. The value of the optical depth of the normal atmosphere along the vertical direction is $\tau \approx 0.1$. The value of the optical depth of the stratosphere is $\tau \leq 0.04$, which is close to the value of common window glass.

A shadow element above a certain region of the eclipsed Moon is characterised by its photometric density D, which is defined as follows:

$$D = -\log B/B_o \qquad [2]$$

where B_o and B are the values of the brightness of the region on the Moon, observed during non-eclipse conditions (the 'Reference Moon') and observed during the eclipse respectively. Link derived the photometric density of the shadow projected on the lunar plane as a function of the distance from the geometrical centre of the shadow.

From Eqn 1 and Eqn 2 it follows:

$$\tau = 2.303\,(\log A + D) \qquad [3]$$

Lunar magnitude

An estimation of the colour and brightness of the Moon during an eclipse is provided by the well-known Danjon index, L. The values of L that have been used in the present analysis are listed in the following catalogues: Stother's catalogue for 68 eclipses between years 1670–1881;[11,12] Link's catalogue which contains the radial profiles of density;[13] the collection of De Vaucouleurs[14] and the collection of Fisher.[15]

When L is the only available index, the magnitude m of the Moon during a total eclipse has been obtained through the following empirical equation:

$$m = 0.263L^2 - 2.72L + 3.55 \qquad [4]$$

This relation stems from a least squares interpolation performed over 62 measures of m and estimates L. Some comments and further statistical properties of the correlation between m and L are represented in Figure 4.

Equation [4] is similar to other polynomial functions already determined by Keen and other researchers, but is based on a larger amount of experimental data. In the present work, equation [4] is used for all the eclipses from 1670 to 1920.

Global optical depth

The integrated luminosity of the Moon during an eclipse represents a useful estimation of the transparency of the terrestrial atmosphere as a whole. We now want to determine a mathematical law to relate the optical depth of the air to the variation of the Moon's luminosity recorded during a total eclipse.

After physical consideration and mathematical development we obtained the equation:

Figure 3. View of the Abruzzo region from the Portella Mountain (Gran Sasso d'Italia) at 2400m above sea level. The vertical pixel value profiles (measured in the RGB channels of the sky digital image) are shown in the plot in the inset. The blue sky is a manifestation of Rayleigh scattering; the white strip above the sea horizon (Adriatic Sea) is caused by forward aerosol scatter. Without scattering the sky would appear black. In the bottom right we can see the dome of the Astronomical Observatory of Rome, and the historic hotel where Benito Mussolini was imprisoned. The vast highland is Campo Imperatore, the 'little Tibet' of Europe: 1800m above sea level. Campo Imperatore is covered by snow for six months of the year. It is a real paradise, in winter for skiers and in summer for amateur astronomers.

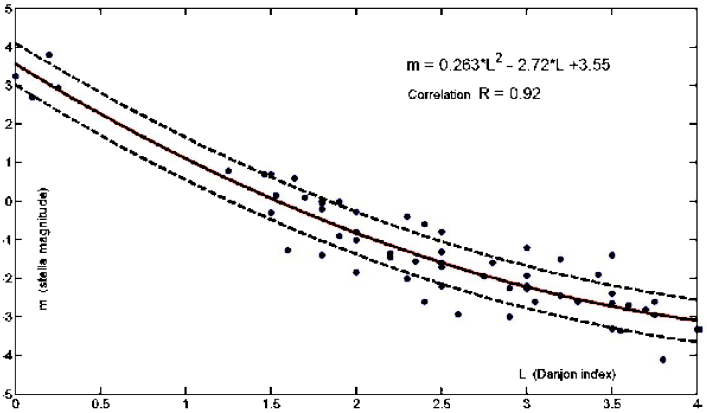

Figure 4. The empirical relationship between the measured integrated lunar magnitude, *m,* (See Table 1) and Danjon's index, *L*. This relation is well represented by a quadratic polynomial (Eqn. 4). 68% of the experimental points are included within the strip between the two dashed curves.

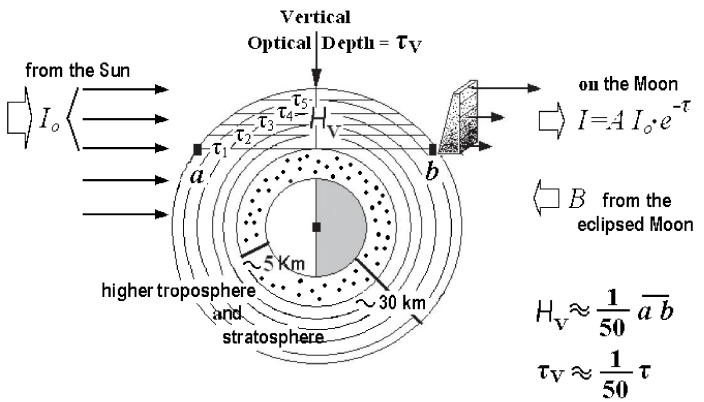

Figure 5. Scheme for calculating a rough value of the atmospheric optical depth, τ_v, along the vertical direction. Here, the Sun is considered as a point source; a–b is the geometrical length (with optical depth, τ) of the ray path tangentially to the base of a thin atmospheric layer. The distance a–b is 50 to 60 times larger than the geometrical vertical thickness H_v (with vertical optical depth τ_v). Let B_o be the observed brightness of the non-eclipsed Moon, proportional to I_o the intensity of direct solar radiation; B is the observed brightness of the eclipsed Moon, proportional to I the intensity of the solar radiation impinging on the eclipsed Moon. The value of τ is calculated from formulae [2] and [3].

$$\tau_V = 0.013(m - m_o) - 0.075 \qquad [5]$$

This represents the medium global optical depth, τ_v, from ~5km upwards along the vertical direction, as a function of the integrated stellar magnitude, *m,* of the Moon during the total maximum phase; $m_o = -12.55$ stands for the integrated magnitude of the non-eclipsed full Moon (*i.e.* the Reference Moon). We estimate the uncertainty on the single values calculated from equation [5] is of the order of 5 to 8%. A simple scheme for an approximate and fast calculation of τ_v is shown in Figure 5.

The ozone layer

The stratosphere includes an ozone layer between about 15km and 35km in altitude. Link suggested that this ozone layer is responsible for the shadow photometric density at about 7 arcmins from the geometric limit of the shadow. Absorption due to ozone is very high in the UV spectral range (Hartley band) and still quite perceivable in the visible (Chappius band). In the visible spectral range, the maximum absorption due to ozone is reached at a wavelength of ~600nm (red-orange).

4.3954	4.3771	4.3011	3.2735	-Int	-Int	-Int	-Int	-Int	-Int
4.3879	4.3823	4.3273	3.9923	-Inf	3.1486	-Inf	-Inf	-Inf	
4.4031	4.3909	4.3641	4.2337	3.2735	-Inf	-Inf	-Inf	-Inf	
4.3941	4.3892	4.3644	4.2827	3.0183	-Inf	-Inf	-Inf	-Inf	
4.3985	4.3862	4.3744	4.3344	3.9927	-Inf	-Inf	-Inf	-Inf	
4.4042	4.3888	4.3756	4.3580	4.1981	-Inf	-Inf	-Inf	-Inf	
4.4016	4.3906	4.3723	4.3617	4.2881	3.5923	-Inf	-Inf	-Inf	
4.4030	4.3913	4.3802	4.3640	4.3177	4.0335	-Inf	-Inf	-Inf	
4.3981	4.3784	4.3648	4.3612	4.3435	4.1562	-Inf	-Inf	3.1709	-Inf
4.3913	4.3776	4.3636	4.3600	4.3522	4.2051	-Inf	-Inf	-Inf	-Inf
4.4007	4.3792	4.3646	4.3580	4.3465	4.2526	2.9056	3.1944	-Inf	-Inf
4.3958	4.3747	4.3724	4.3491	4.3481	4.2685	3.7835	-Inf	-Inf	-Inf
4.3873	4.3616	4.3606	4.3551	4.3415	4.2735	3.9783	-Inf	3.1709	-Inf
4.3854	4.3668	4.3527	4.3510	4.3343	4.2915	4.0676	3.3357	-Inf	-Inf
4.3731	4.3670	4.3662	4.3447	4.3364	4.3026	4.1289	-Inf	3.1486	-Inf
4.3753	4.3670	4.3569	4.3434	4.3348	4.3053	4.1036	-Inf	-Inf	3.1274
4.3688	4.3625	4.3509	4.3481	4.3262	4.3010	4.0940	-Inf	-Inf	-Inf
4.3662	4.3562	4.3476	4.3431	4.3269	4.3159	4.1517	-Inf	-Inf	-Inf
4.3779	4.3660	4.3510	4.3341	4.3303	4.3094	4.1486	-Inf	-Inf	3.1486
4.3664	4.3612	4.3522	4.3377	4.3218	4.3089	4.0727	-Inf	3.1072	-Inf
4.3633	4.3607	4.3414	4.3326	4.3132	4.2961	4.0780	-Inf	-Inf	-Inf
4.3627	4.3556	4.3437	4.3247	4.3093	4.2839	4.0279	-Inf	-Inf	-Inf
4.3574	4.3451	4.3366	4.3218	4.3151	4.2716	3.9249	-Inf	-Inf	-Inf
4.3440	4.3415	4.3336	4.3182	4.3113	4.2528	3.4584	-Inf	-Inf	-Inf
4.3385	4.3411	4.3247	4.3085	4.3221	4.1985	3.3357	-Inf	-Inf	-Inf
4.3464	4.3350	4.3196	4.3116	4.3099	4.1280	3.3357	-Inf	-Inf	-Inf
4.3395	4.3291	4.3155	4.3164	4.2773	3.9768	-Inf	-Inf	-Inf	-Inf
4.3399	4.3211	4.3121	4.3091	4.2378	3.6045	-Inf	-Inf	-Inf	-Inf
4.3372	4.3185	4.3064	4.3043	4.1679	-Inf	-Inf	-Inf	-Inf	-Inf
4.3295	4.3213	4.3080	4.2827	3.9915	-Inf	-Inf	-Inf	-Inf	-Inf
4.3300	4.3172	4.3118	4.2196	3.3615	-Inf	-Inf	-Inf	-Inf	-Inf
4.3319	4.3067	4.3012	4.1138	3.3357	-Inf	-Inf	-Inf	-Inf	-Inf
4.3160	4.3174	4.2504	3.6938	3.3035	-Inf	-Inf	-Inf	-Inf	-Inf
4.3106	4.2996	4.1230	3.2455	3.4496	-Inf	-Inf	-Inf	-Inf	-Inf
4.3234	4.2447	3.6862	3.3705	3.1072	-Inf	-Inf	-Inf	-Inf	-Inf
4.2947	4.0872	-Inf	-Inf	-Inf	-Inf	-Inf	-Inf	-Inf	-Inf
4.1934	2.8933	-Inf	-Inf	-Inf	-Inf	-Inf	-Inf	-Inf	-Inf
3.8968	3.3035	-Inf	-Inf	-Inf	-Inf	-Inf	-Inf	-Inf	-Inf
3.2455	-Inf	-Inf	-Inf	-Inf	-Inf	-Inf	-Inf	-Inf	-Inf
-Inf	-Inf	-Inf	-Inf	-Inf	-Inf	-Inf	-Inf	-Inf	-Inf

Figure 6. Bi-dimensional numerical matrix with the density values as entries, given by the MATLAB software. This is from the Red channel component of an eclipsed Lunar image. –Inf is for Density= 0. The outline of the Moon is very well defined.

Between 1910 and 1920, Fabry & Buisson performed numerous measurements of ozone (O_3) in the atmosphere.[16] Since then, eclipse photometry has also been applied to reveal the presence of this atmospheric component.[17]

Link computed the photometric density [2] as a function of the distance from the shadow centre, without including the effect of ozone. Thus, the difference (D_O–D_C) between the observed photometric density, D_O, and the computed density, D_C, detected in

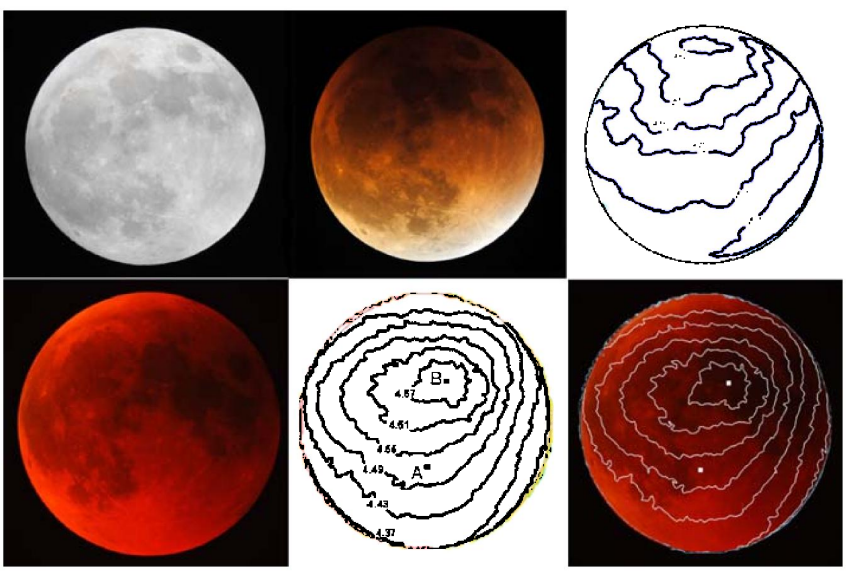

Figure 7. Isophotes are lines along which the photometric density has a constant value. Top: Reference Moon, eclipse of 2015 September 28 and isophotes. Bottom: images and isophotes of the eclipse of 2011 June 15. Point A is the geometric centre of the umbra, point B is the maximum density of the umbra. At least one image of the Reference Moon is needed to study the eclipse phenomenon.

the red part of the spectrum at ~7' from the umbra edge, depends exclusively on the total quantity of O_3 present in the stratosphere.

Therefore, we present an analytical formula to compute both the numerical density (expressed in molecules/m^3) and the ozone layer thickness (expressed in Dobson units) as a function of the difference (D_O–D_C).

After physical considerations and many tedious analytical steps, which for simplicity and clarity it is not appropriate to show here, we obtained the following two formulae:

$$N_o = 5.7\times10^{18}\Delta \quad [6]$$

$$S = 380\,\Delta \quad [7]$$

where N_o is the maximum volume number density of O_3 (molecules/m^3), S is the layer thickness in Dobson units (DU) and the numerical factor $\Delta = 2.3(D_O - D_C)$ is taken at ~7 arcmin from the umbra edge.

We refer to Equations 4 to 7 as the *Formulae of Colle Leone* (from now on, 'FCL'), as the present work has been conducted at the Colle Leone Astronomical Observatory located in central Italy (MPC observatory code C96; *OACL.net*). The uncertainty in the values given by the FCL depends on the accuracy of the values of the constants, which have been theoretically determined.

Experimental procedure

The experimental technique compares the brightness of a lunar region during an eclipse with the same region out of eclipse. Through the use of commercial software (*Photoshop*), the image of the non-eclipsed Moon (Reference Moon) is made superimposable and hence comparable to the image of the Moon during the eclipse.[18] Subsequently, we read (using MATLAB software) the pixel values (PV) of each image. The PV of a non-saturated pixel is proportional to the exposure duration and to the brightness of the part of the Moon represented by the pixel itself.[19] Therefore, for each pixel of the image of the eclipsed Moon the photometric density can easily be obtained.

Afterwards, all the PVs that are read in each of the three spectral ranges, RG & B, (*i.e.* the RGB channels of the image) are reduced to the same exposure time and to the same zenith angle of the Reference Moon. In this way, for each spectral band of the image there is a corresponding bi-dimensional numerical matrix with the density values as entries (Figure 6). At this point, each matrix can be manipulated mathematically.

Figure 7 represents the isophote curves of the shadow in the R band for two recent total eclipses. Figure 8 shows the isophotes in the umbra and penumbra during a partial eclipse. Both in the external and in the inner shadow, the isophote curves are irregular, this irregularity being ascribable to the non-homogeneity of the atmosphere. The inner curves assume an elliptical shape, stretched and centred on about 10' from the geometric centre of the shadow. The shape,

Table 1. Lunar eclipses and large volcanic eruptions, 1703–2015

The Atmospheric Optical Depth τ_v obtained from 104 lunar eclipses since 1703 and large volcanic eruptions with a VEI (Volcanic Explosive Index) of 4 or more. m is the stellar magnitude of the eclipsed Moon (*= measured values), L is Danjon's number from qualitative observations. This list omits several eclipses due to lack of useful data. Some eruptions were contemporaneous with others not listed here. n indicates the eruption as noted on Figure 9.

Eclipse	*m*	*L*	τ_v	*Volcano*	*Location*	*Start date*	*n*
1703 Dec 23	−0.49	1.8	0.082	Long Is	New Guinea	1703 ?	(1)
1729 Aug 09	+2.6	1.4	0.09	Oraefajokull	Iceland	1727-28	(2)
1761 May 18	+1.09	1	0.104	Makian	Indonesia	1760 Sep	(3)
1787 Jan 03	−1.42	2.37	0.069	Laki	Iceland	1784	(4)
1816 June 16	+2.26	0.5	0.117	Tambora	Indonesia	1815 Apr	(5)
1826 May 21	+0.06	1.5	0.089	Isanotski	Aleutin Is	1825 Mar	(6)
1856 Oct 13	−2.46	3.2	0.056				
1873 Sept 04	−0.84	2	0.077	Grimsvotn	Iceland	1873 Jan	(7)
1884 Oct 04	+2.5	0.5	0.12	Krakatau	Indonesia	1883 Aug	(8)
1888 Jan 28	−2.75	3.35	0.05				
1891 Nov 15	−2.5	3.25	0.055				
1892 Nov 04	−0.5	1.8	0.08				
1895 Mar 10	−1.95	2.75	0.065				
1895 Sept 04	−0.5	1.8	0.08				
1896 Feb 28	−1.75	2.6	0.065				
1898 July 03	−2.25	3	0.055				
1898 Dec 27	−2.6	3.25	0.054				
1899 Dec 16	−2.7	3.4	0.053				
1902 Apr 22	−1.3	2.3	0.071				
1903 Apr 12	+2.5	0.4	0.12	Mont Pelée	Martinica	1902 May	(9)
1903 Oct 06	+3.55	0	0.134	Sant Maria	Guatemala	1902–1904	(10)
1906 Feb 09	−1.6	2.5	0.067				
1906 Aug 04	−0.85	2	0.077				
1909 June 03	−2.8	3.5	0.05				
1909 Nov 27	−1.5	2.5	0.07				
1910 Nov 16	−2.25	3	0.060				
1913 Mar 21	+1.45	0.85	0.107	Katmai	Alaska	1912 Jun	(11)
1914 Mar 12	−1.25	2.25	0.072				
1917 July 04	−1.9	2.7	0.063				
1920 May 03	−1.2*	3	0.073				
1921 Oct 16	−2.8*	3.7	0.052				
1924 Feb 20	+1.0	1	0.10	Raikoke	Kurile Is.	1924 Feb	(12)
1924 Aug 14	−2.65*	2.5	0.055				
1927 Dec 08	−1.6*	2.6	0.067				
1928 Nov 27	−2.5*	3.5	0.056				
1931 May 02	−0.8*	3.4	0.078				
1931 Sept 26	−2.8*	3.6	0.053				
1932 Sept 14	−2.7*	3.4	0.052	Fuego	Guatemala	1932 Jan	(13)
1935 Jan 19	+2.25	0.5	0.12				
1936 Jan 08	−3.3*	3.5	0.045				
1938 Nov 07	−2*	2.3	0.062				
1942 Mar 02	−0.6*	2	0.080				
1942 Aug 26	−1.6*	3.25	0.067				
1943 Feb 20	−2.9*	3.6	0.05				
1943 Aug 15	−2.95	3.75	0.05				
1945 Dec 18	+0.06	1.5	0.09	Kliuchevskoi	Kamchatka	1945 Jan	(14)
1946 Dec 08	−1.6	2.5	0.067				
1949 Apr 13	−1.3*	2.3	0.070				
1949 Oct 07	−1.94	2.75	0.063				
1950 Apr 02	−2.6*	3.75	0.054				
1950 Sept 26	−4.25*	3.8	0.033				
1953 Jan 29	−1.4*	3.5	0.07				
1953 July 26	+0.40	1.3	0.093	Mt Spurr	Alaska	1953 Jul	(15)
1954 Jan 19	−0.5*	2.5	0.082				
1956 Nov 18	−1.35*	2.2	0.07	Bezymyannaya	Kamchatka	1956 Mar	(16)
1957 May 13	−0.1*	1.5	0.087				
1957 Nov 07	+0.6	1.5	0.09				
1960 Mar 13	−0.9*	1.9	0.076				
1960 Sept 05	−0.05*	1.8	0.087				
1961 Aug 26	−2.2*	2.5	0.06				
1963 Dec 30	+3.85*	0.2	0.138	Agung	Bali	1963 Mar	(17)
1964 Jun 25	+2.4*	0.0	0.12				
1964 Dec 19	+0.1*	1.7	0.090				
1967 Apr 24	−0.8*	2	0.078				
1967 Oct 18	−1.5*	3.2	0.069				
1968 Apr 13	−2.75*	2.5	0.052				
1968 Oct 06	−0.13	1.6	0.08	Fernandina Is.	Galapagos	1968 Jun	(18)
1971 Feb 10	−1.8*	2.6	0.065				
1971 Aug 06	0.0*	1.6	0.088				
1972 Jan 30	−3.*	3.75	0.050				
1974 Nov 29	−1.7*	2.5	0.066				
1975 May 25	+0.6*	1.8	0.096	Fuego	Guatemala	1974 Oct	(19)

Table 1. *(continued)*

Eclipse	*m*	*L*	τ_v	*Volcano*	*Location*	*Start date*	*n*
1975 Nov 18	−2.95*	2.6	0.05				
1978 Mar 24	−1.*	2	0.062				
1978 Sept 16	−1.45*	2.2	0.069				
1979 Sept 06	−1.8*	3	0.065				
1982 Jan 09	−2.25*	3	0.059				
1982 July 06	+0.7*	1.45	0.088				
1982 Dec 30	+3.*	0.25	0.127	El Chichon	Mexico	1982 Apr	(20)
1985 May 04	0.0*	1.5	0.088				
1985 Oct 28	−2.2	3	0.06				
1986 Oct 17	−1.7	2.6	0.066				
1989 Aug 17	0.6	1.5	0.09				
1990 Feb 09	−3.30*	4	0.050				
1992 Dec 09	+3.25*	0	0.13	Mt Pinatubo	Philippines	1991 Jun	(21)
1993 June 04	−1.*	2	0.075				
1993 Nov 29	−1.3*	2.5	0.071				
1996 Apr 04	−1.6	2.5	0.067				
1996 Sept 27	−1.9	2.7	0.063				
1997 Sept 16	−1.9*	3.4	0.063				
2000 Jan 21	−1.85*	1.9	0.064				
2001 Jan 09	−1.5*	2.5	0.07				
2003 May 16	−0.5*	1.8	0.082	Reventador	Ecuador	2002 Nov	(22)
2003 Nov 08	−2.5*	3.5	0.056				
2004 May 04	−2.6*	3.3	0.054				
2004 Oct 28	−2.2*	2.5	0.060				
2007 Mar 03	−1.6*	1.8	0.067				
2007 Aug 28	−2.	2.8	0.062				
2008 Feb 21	−2.45*	3.2	0.056				
2011 June 15	−0.3*	1.25	0.084	Grimsvotn	Iceland	2011 May	(23)
2011 Dec 10	−2.45*	3.2	0.056				
2014 Apr 14	−1.62*	2.5	0.067				
2014 Oct 08	−2.27*	3	0.06				
2015 Sept 28	+0.8*	1.25	0.1	Calbuco	Chile	2015 Apr	(24)

position and values of these isophotes mainly depend on the physical conditions in the troposphere.

Practical results

Volcanic emissions in the stratosphere

The integrated luminosity of the Moon during an eclipse represents a useful estimation of the transparency of the terrestrial atmosphere as a whole. In this context, lunar eclipses have previously been used as aerological indicators.[20–24]

In 1987 Richard Keen (Colorado University) computed the optical depth of the stratosphere by using values of the Moon's luminosity registered in 21 different eclipses, which occurred between 1960 and 1986.[25,26] Keen found a strong correlation between volcanic eruptions and the increase in the optical depth of the stratosphere on a planetary scale.

The following analysis was conducted on the basis of 164 eclipses between 1670 and 2015. The phenomena between 1884 and 2015 (and some others since 1703) are included in Table 1.

Figure 9 shows the global optical depth, τ_V, for more than three centuries, from 1670 to 2015. The τ_V values, calculated via FCL eqn [5] and their time distribution, are in good agreement with the results obtained by other authors through methods based on the chemical analysis of polar ice samples and tree rings.[27–30] The marks on the top of the figure indicate the epochs of great volcanic eruptions (Table 1, column 5).

There is strong evidence for an increase in τ_V (*i.e.* a reduction of the stratospheric transparency) following major volcanic eruptions. Some examples are presented in the following paragraphs.

From the analysis of the eclipse in the year 1884, a large optical depth equal to 0.12 is found. This eclipse occurred just after the enormous volcanic explosion of Krakatoa in 1883. The following are also of particular interest:

i) $\tau_V = 0.119$, obtained from the eclipse after the famous eruption of Tambora, in Indonesia, in 1815;

ii) $\tau_V = 0.13$, obtained from the eclipse which followed the lesser known volcanic eruption of Santa Maria in 1902 June.

The eruption of the El Chichon volcano in 1982 April was the subject of several studies. In this case, FCL[5] provides $\tau_V = 0.13$, which matches the range of values 0.04–0.15 measured at several global observatories (LIDAR stations) during the following October. The eruption of Mt Pinatubo in 1991 June was one of the major eruptions in the 20th century. The first total eclipse after the eruption occurred 18 months later, which is similar to the usual settling

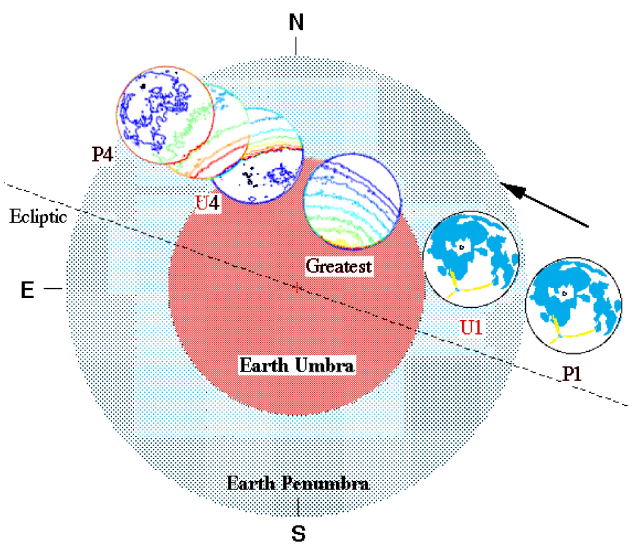

Figure 8. Partial eclipse of 2008 August 16, showing isophotes of the umbra and penumbra. Pollution by human activity is very limited in the stratosphere. Ozone absorbs in the visible band more than all the other molecular and atomic species present in the stratosphere. Therefore, the photometric density of the umbra around 7 arcmin from the edge can be nearly all attributed to the ozone layer.

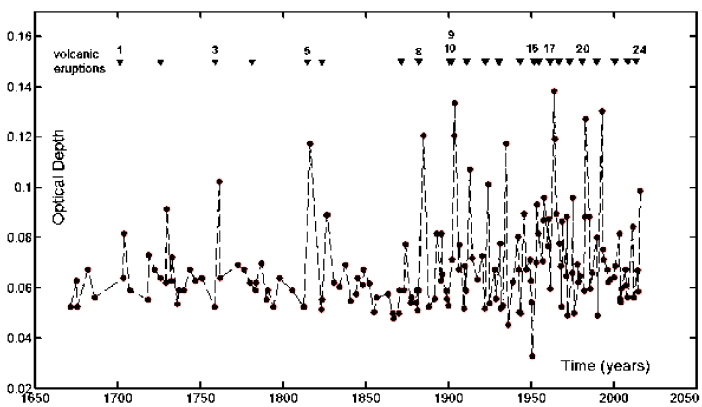

Figure 9. Variation of atmospheric optical depth from 1670 to 2015, calculated from Colle Leone Formula [5] and observational data of 164 eclipses. The times of the great volcanic eruptions (Table 1) are indicated by triangles & sequential numbers (last column of Table 1). All eclipses after a great eruption have been less bright than those that occurred well away from eruptions. To the untutored eye it seems that the increase of atmospheric opacity might be due to anthropogenic effects (see Figure 11) and more frequent around great volcanic eruptions.

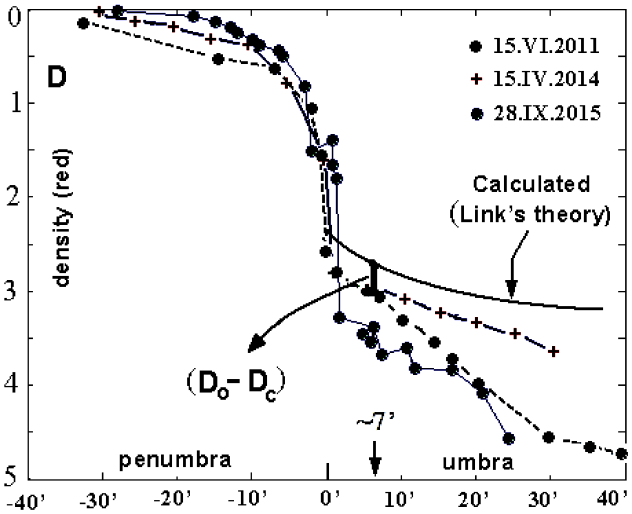

Figure 10. Photometric density profiles along a radius inside the umbra, calculated and observed during three total eclipses: 2011 June 15 and 2014 April 14 (Colle Leone Obs.); 2015 September 28 (Cochise Sky Obs., Arizona). The umbra edge lies on the inflection point of the observed profile. Inside the penumbra the calculated and observed densities almost coincide.

time of volcanic particles released in the stratosphere, but still gave a very large value of $\tau_V = 0.13$.

In summary, the method based on lunar eclipses highlights a strong correlation between the lower values of atmospheric transparency *(i.e.* high τ_V) and volcanic eruptions. In other words, eclipses occurring up to 2 years after a great eruption are more likely to be dark eclipses. In addition there is some evidence for an increased frequency of volcanic eruptions during the 20th century and an associated increase in τ_V.

Isophotes and ozone

Figure 10 shows the radial profiles of the photometric densities in the R band registered during three recent eclipses. A comparison can be made with the profile of D as computed by Link. We notice that the values of the computed densities are smaller than the values of the observed ones. The value $\Delta \approx 0.65$ (eclipse of 2011 June 15), was detected at ~7 arcmin from the shadow limit. The FCL nos. [6] & [7] provide, respectively, a maximum number density $N_o = 3.7\times10^{18}$m^{-3} and a thickness S= 247 DU of the ozone layer at the mean latitude of the terminator arc involved in the phenomenon.

Table 2 presents the values of Δ for 11 eclipses and the corresponding values of the ozone layer thickness given by equation [7]. (Unfortunately there are insufficient data for other eclipses). These values are compared with those published in the geophysical literature during the corresponding period.[31–35] At low latitude, where the ozone layer is relatively constant in thickness, the mean value from the technique is about ~200 DU compared to ~240 DU from satellite measurements. At higher latitudes the seasonal variation in thickness varies from around 280 DU in the autumn to over 400 DU in the spring when measured by satellite, and here the mean value for the thickness from the technique is ~340 DU.

The thickness values, *S,* from the eclipses of 1954 Jan 18 and 2015 Sep 28 in particular are larger than the normal values measured at equatorial and temperate latitudes. The large values for the difference (D_O–D_C) are presumably due to the presence in the stratosphere of dusts and microgranules (or aerosols) released by the great explosions of Mt Spurr in Alaska, which occurred in 1953 June, six months before the 1954 eclipse, and of the Calbuco volcano in Chile in 2015 April.

In the case of the 1954 July 15 eclipse, one year after the eruption of Mt Spurr, the thickness of the ozone layer at middle-high latitudes was about ~315 DU. Similar considerations hold true for the eclipse of 1943 Feb 20; the FCL [7] gives a thickness S≈ 300 DU, whilst the value measured at the ozone observatory at Arosa in Switzerland was S≈ 320 DU. During more recent eclipses, the ozone layer thickness from FCL [7] matches with the direct measurements from satellite and ground based observatories.

We focus the present analysis on a limited number of phenomena, mainly because of the lack of data. However, the results suggest that Equation [7] may represent a tool to approximate the quantity of ozone in the stratosphere, especially in the past, when direct measurements of ozone were not conducted systematically. A proviso is that only eclipses that occurred well away from major volcanic eruptions should be used in such determinations.

Table 2. Atmospheric calculations using the lunar eclipses method

Number density of molecules, N_o, and ozone layer thickness, *S,* (Dobson Units) calculated with the lunar eclipses method; c= rising phase, d=decreasing phase. Values for S_m are taken from published geophysical literature. The uncertainty in *S* is ≈10%, or greater. It is very difficult to take into account a perturbing factor, such as volcanic aerosols, *e.g.* the recent estimate from the eclipse of 2015 Sept 28. The large gap between 1954 and 2001 is due to a lack of images of the reference Moon in the eclipse observations, or of ozone data.

Eclipse		*Δ*	*N_o×10^{18}/m^3*	*S(DU)*	*S_m(DU)*	*Lat. of terminator arc*
1932 Sept 14	c	0.48	2.7	182	310	−1°
	d	0.85	4.8	323	310	+57°
1938 Nov 07		0.80	4.6	304	300	+30°
1943 Feb 20		0.79	4.5	300	320	+50°
1953 Jan 29	c	0.87	4.9	330	310	+57°
	d	0.52	3.0	198	310	+6°
1954 Jan 19	c	0.97	5.5	369	no data	−9°
	d	1.09	6.2	414	no data	−44°
1954 Jul 15	c	0.82	4.5	312	340	+36°
	d	0.83	4.7	315	340	+56°
2001 Jan 09		1.10	6.3	418	325	+55°
2008 Aug 16		0.90	5.0	342	330	+65°
2011 June 15	c	0.62	3.5	236	270	+8°
	d	0.67	3.8	255	270	+30°
2014 Apr 15	c	0.64	3.6	243	240	−30°
2015 Sept 28	d	1.80	10.3	684	320	−35°

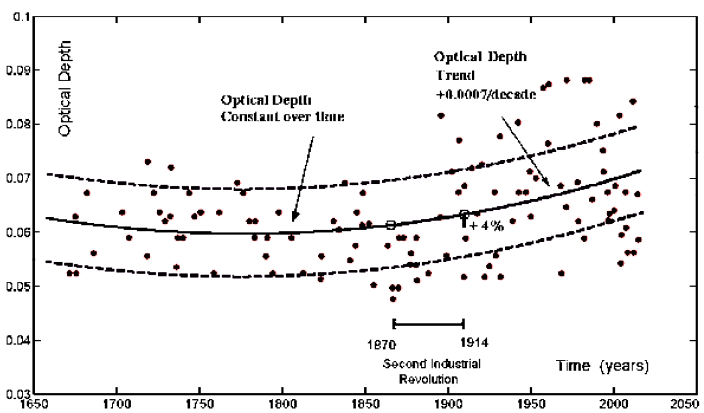

Figure 11. Optical depth time series with a best-fit (least squares) parabolic trend. When computing the curve (solid line), values with optical depth $\tau_v \geq 0.09$, associated with great volcanic eruptions, were excluded. The trend may be increasing because of human activities and more frequent volcanic eruptions.

Optical depth and human activities

Without considering the spikes of τ_V corresponding to volcanic eruptions, it is possible to split the time trends of the stratospheric optical depth into two main intervals (Figure 11): a first interval with a mean value of $\tau_V \approx 0.061$, extending until 1870, and a second one, from 1915 onwards.

From the decade 1870–1880 onwards, the values start increasing, until they reach a value around $\tau_V = 0.068$, which corresponds to the present-day situation. This growth might be due to the growing concentration of aerosols and greenhouse gases, which have been continuously released into the atmosphere since the beginning of the so-called Second Industrial Revolution, the phase of rapid industrialisation in the final third of the 19th century and the beginning of the 20th.[36] However, we must caution against a definite conclusion as this period also seems to have suffered an increased frequency of volcanic eruptions.

An increase of the optical depth of about 0.007 can be considered as little variation, however the attenuation of solar radiation transmitted by the layer to the Earth's surface undergoes a change of ~0.7%. This is higher than the variation ~0.1% of the solar irradiance during a whole sunspot cycle and so could have a climatic impact. These two variations can be distinguished only with the help of highly accurate satellite measurements. Over the present study period (1870 onwards), the changes due to anthropogenic effects are constantly increasing.

Optical depth and the solar cycle

In 1920 André Danjon presented an empirical law, which states that the variation of brightness and the colouring of the eclipsed Moon is a function of the variation in solar activity: dark eclipses occur in the two years following the minimum numbers of sunspots in the solar cycle and bright eclipses occur just before their maximum.[37,38]

This 'law' was immediately disproved in 1921 by E. Walter Maunder, in an article in the *JBAA*.[39] Danjon's law has not subsequently been confirmed.

In an attempt to find a minimal hypothetical link between the global atmospheric optical depth and solar activity, we looked for a possible statistical correlation between variations of τ_V and the annual average of the Wolf numbers, and solar cycle phase. The Wolf number is a quantity that measures the number of sunspots and groups of sunspots observed on the surface of the Sun.

Such correlations do not appear to exist, as can be seen in Figure 12. Furthermore, the values of τ_V and the values of the solar irradiance seem to be independent of one another. Intuitively, it is very unlikely that the small oscillation of the irradiance values (~0.1%) could induce a variation of some stellar magnitudes in eclipse brightness. That is, the present study does not even partially confirm Danjon's law. On the other hand, no analogy can be observed with the more obvious Maunder minimum (1645–1715) in solar activity.

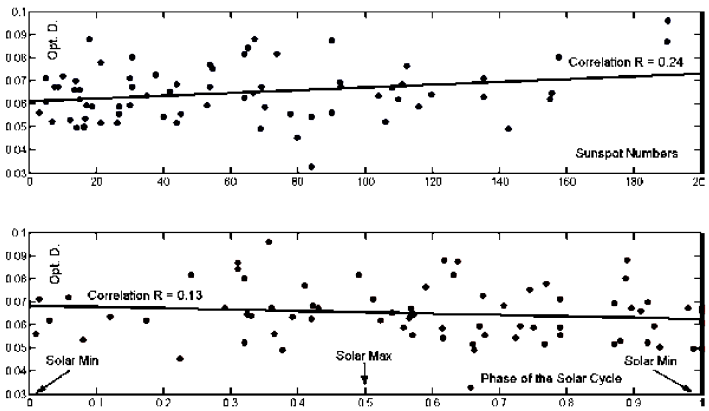

Figure 12. Optical depth, plotted against sunspot Wolf number (upper diagram), and phase of the solar cycle (bottom diagram). The best fitting straight lines are nearly parallel to the abscissa. The correlation coefficient R≈ 0.2 indicates that there is no statistical relationship between the transparency of the air and solar activity.

Conclusions

The results of the present analysis confirm that the variation of the terrestrial atmospheric transparency only depends on causes intrinsic to our planet, and in particular on volcanic activity and perhaps human activity over the last ~150 years. FCL [4] and [5] establish a quantitative relation between the vertical optical depth τ_V and the subjective index, *L,* of Danjon. While the method of eclipses has a poor time resolution, mainly because a total lunar eclipse occurs on average only once a year, and requires photometric measurements as well as good descriptions of the eclipse, it does allow derivation of useful quantitative information concerning the atmosphere. It provides an overall picture of atmospheric pollution, particularly in past times with no instrumental measurements. This analysis is very important in order to detect atmospheric variations on century time scales.

Photometry of lunar eclipses shows that in the stratosphere aerosols have increased over the last century and that they take rather a long time to settle. Such aerosols contribute to light pollution in our skies through backscatter, and now make a significant contribution to this phenomenon which is perhaps inexorable and irreversible.

Acknowledgments

The author is most grateful to Jonathan Shanklin (joint discoverer of the Antarctic ozone hole) who has patiently improved this work. He also thanks Dr Jeremy Shears (then President of the BAA) who made many suggestions. I am indebted to Prof Bob Gent (President of the International Dark-Sky Association) who carried out observations from Cochise Skies Observatory, Arizona. Particular thanks to my son Antonio (Technical University of Munich), with whom I have discussed many mathematical and physical matters. Thanks also to Alberto Martos (Agrupacion Astronómica de Madrid), Maurizio Locatelli, Pierluigi Pasqualone and Benedetto Chinaglia (Italian amateur astronomers) who provided their own observations of some eclipses.

Address: Osservatorio Astronomico di Colle Leone (OACL.net) Mosciano Santangelo (Teramo), Italy. [*miracat@tin.it*]

References

1 Link M. F., *Bull. Astr.*, **8**, 77 (1933)
2 Link M. F., *Adv. Astron. Astrophys.* **2**, 87 (1963)

Frank Wilsenham Hyde (1909–1984): Radio astronomer extraordinaire!

Martin Mobberley

Frank Wilsenham Hyde was a popular character in the BAA from 1957 to 1966, receiving the Association's Merlin Medal in 1963 and serving briefly as the Editor of the *Journal* from 1963 November to 1965 December. His extraordinary Radio Astronomy Observatory was the most advanced amateur facility in the UK during the 1960s, and the media even described it as 'a miniature Jodrell Bank'. However, increasing financial problems led to his dramatic exit from the Association and the dismantling of his observatory in 1967.

Frank Wilsenham Hyde (Figure 1) was born in Rochford, near Southend-on-Sea, on 1909 March 10. As a young man he became interested in electronics and in his twenties he began to dabble with radio astronomy from his back garden, even before the start of World War II. His early interest was inspired by hearing about the pioneering work of Karl Jansky in 1932, and also that of Grote Reber.

After the war ended, in 1945, Hyde's interest in the subject resumed. At that time he worked for the electronics company Crompton–Parkinson at their Writtle Road site in Chelmsford. With the technological advances in electronics made during the war years, there was a growing interest in carrying out radio astronomy after the conflict had ended and Hyde was at the forefront of the amateur effort, while the names of Bernard Lovell, Martin Ryle, Anthony Hewish and a few others spearheaded the professional approach.

In the first ten or so years after World War II Hyde carried out radio astronomy from the back garden of his Clacton home at 27 Carlton Road (Figure 2). However, he had much bigger plans, and wanted to set up a large interferometer (superposing waves from multiple aerials) working at 27MHz as well as using his smaller 240MHz aerials. The lower frequency meant a longer wavelength and far more space than a back garden could provide, especially when an interferometer was planned. He also wanted to move further away from the sources of interference experienced in a normal street of houses. So, in the late 1950s Hyde started laying his antennae out on deserted marshland at nearby St Osyth, using his caravan as a control room and achieving baselines (aerial separation) of 1,000 feet (305m).

Figure 1. Frank Hyde in the 1960s, from a *Look at Life* cinema newsreel.

By this time Hyde had long since parted company with his day job in Chelmsford and planned to use his expertise to set up a radio and television dealership in Clacton. In post-war Britain, renting, selling and maintaining televisions and radios was a booming business and Hyde understood the tech-

▶ *Di Giovanni: Lunar eclipse brightness and the terrestrial atmosphere (continued)*

3 Link M .F., *Eclipses Phenomena*, Springer Berlin (1969)
4 Garcia Munoz M. & Pallé E., *JQSRT doi:10,1016/j.jqrst. 2011.03.17*
5 Hernitsche K. N. *et al.*, *Appl. Opt.*, **47**, 34, H62 (2008)
6 Vollmer M. & Geldzelman S. D., *ibid.*, **47**, 34, H52 (2008)
7 Gedzelman S. D. & Vollmer M., *ibid.*, **47**, 34, H1149 (2008)
8 Theodore C. Y. & Cutler B., *Geophys. Interfaces* (2009)
9 Visconti G., *Fundamentals of Physics & Chemistry of Atmosphere*, Springer–Verlag, Berlin, 2001
10 Sanchez–Lavega A., *An Introduction to Planetary Atmospheres,* CRC Press, London, 2011
11 Stother R. B., *PASP*, **116**, 886 (2004 Sept)
12 Stother R. B., *ibid.*, **117**,1445 (2005 Dec)
13 Link M. F., *Publ. Obs. Prague* **29** (1956): **http://www.asu.cas.cz/~publ/PAICz029/PAI29.pdf**
14 De Vaucouleurs G., *Comptes Rendus Acad. Paris*, **218**, 655 (1944): **http://gallica.bnf.fr/ark:/12148/bpt6k3124m/f1127.image**
15 Fisher W. J., *Smithson. Mis. Collec.*, **76**, 61, 2751 (1924): **http://biostor.org/display_journal.php?oclc=1376204**
16a Fabry C. & Buisson H., *J.Phys. Rad. Série* **5**(3), 196 (1913)
16b Fabry C. & Buisson H., *ibid.,* **6**(2), 197 (1921)
17 Ugolnikov O. S. & Malkov I. A., *Atmos. Oceanic Opt.*, **22**, 365 (2009)
18 Nakamura T. *et al.*, *EM&P* **35**, 55 (1986)
19 Berry E. & Burnell J., *Astronomical Image Processing,* William–Bell, Richmond, USA, 2000
20 Fischer W. J., *Pop. Astron.* **32**, 288 (1924)
21 Fesekov V. G., *Soviet Astron.*, **14**, 195 (1970)
22 Link M. F., *The Moon*, **11**, 261 (1974)
23 Ugolnikov O. S. & Maslov I. A., *Phys. Auroral Phenom., Proc. XXXII Ann. Seminary*, 211 (2009)
24 Ugolnikov O. S., *YSC'16 Proceedings*
25a Keen R., *Science*, **222**, 1011–1013 (1983)
25b Keen R., **lasp.colorado.edu/sorce/news/2008ScienceMeeting/**
25c Keen R., *Bull. Global Volcanism Netw.*, **18**(2), 15–16 (1993 Feb 28)
26 Hoffman D. *et al., Volcanism Earth's Atmosphere Geophysical Monograph* 139 (2009)
27 Stother R. B., *J. Brit. Astron. Assoc.,* **96**, 95 (1986)
28 **http://www.geo.umass.edu/faculty/bradley/bradly1992b.pdf**
29 Christia D., Schomwiese, *Atmosphera* **1**, 141 (1988)
30 Sato M. & Hansen J. E., *JGR* **98**, D12,22.987 Dec (1993)
31 Bronnimann S. *et al.*, *Q.J.R. Meteorol. Soc.,* **129**, 2797 (2003)
32 Bronnimann S. *et al.*, *ibid.*, **129**, 2819 (2003)
33 **www.atmos-chem-phys-discuss.net/6/3913/2006/**
34 L. Kaare *Geof. Publ.*, **18**(6), 5 (1952?)
35 **http://exp-studies.tor.ec.gc.ca/cgi-bin/selectMap**
36 Charlson R. J. *et al.*, *Science* **255**, 423 (1992)
37a Danjon A., *Comptes Rendus Acad. Sci.*, t.171, 1127 (1920)
37b Danjon A., *ibid.*, t.171, 1207 (1920)
38 **http://gallica.bnf.fr/ark:/12148/bpt6k3124m/f1127.image**
39 Maunder W., *J. Brit. Astron. Assoc.*, **31**, 346 (1921)

*[The numerical data used in this report are scattered over many journals of astronomy and geophysics, available in the digital library SAO/NASA ADS (**http://adswww.harvard.edu/**)]*

Received 2016 August 12; accepted 2017 January 21